Lack of TRF2 in ALT cells causes PML-dependent p53 activation and loss of telomeric DNA

Martina Stagno D'Alcontres,[1] Aaron Mendez-Bermudez,[2] Jennifer L. Foxon,[2] Nicola J. Royle,[2] and Paolo Salomoni[1]

[1]MRC Toxicology Unit, University of Leicester, Leicester LE1 9HN, England, UK
[2]Department of Genetics, University of Leicester, Leicester LE1 7RH, England, UK

Alternative lengthening of telomere (ALT) tumors maintain telomeres by a telomerase-independent mechanism and are characterized by a nuclear structure called the ALT-associated PML body (APB). TRF2 is a component of a telomeric DNA/protein complex called shelterin. However, TRF2 function in ALT cells remains elusive. In telomerase-positive tumor cells, TRF2 inactivation results in telomere de-protection, activation of ATM, and consequent induction of p53-dependent apoptosis. We show that in ALT cells this sequence of events is different. First, TRF2 inactivation/silencing does not induce cell death in p53-proficient ALT cells, but rather triggers cellular senescence. Second, ATM is constitutively activated in ALT cells and colocalizes with TRF2 into APBs. However, it is only following TRF2 silencing that the ATM target p53 is activated. In this context, PML is indispensable for p53-dependent p21 induction. Finally, we find a substantial loss of telomeric DNA upon stable TRF2 knockdown in ALT cells. Overall, we provide insight into the functional consequences of shelterin alterations in ALT cells.

Introduction

The majority of human tumors maintain indefinite replicative potential through the activation of telomerase. Although telomerase activity is the more common mechanism used to maintain telomeres, a number of tumors, tumor-derived, and in vitro–immortalized cell lines have been shown to maintain telomeres in the absence of telomerase. These cells use a recombination-based mechanism that has been termed alternative lengthening of telomeres (ALT) (Bryan et al., 1995). In particular, ALT tumors mainly include specific subtypes of soft tissue sarcomas associated with complex karyotypes, astrocytic brain tumors and osteosarcomas (Muntoni and Reddel, 2005).

The onset of ALT is determined by the appearance of heterogenous telomere length, high rates of telomeric sister chromatid exchange (T-SCE) (Londono-Vallejo et al., 2004), the presence of extra-chromosomal telomeric DNA, and the appearance of ALT–associated promyelocytic leukemia bodies (APBs) (Yeager et al., 1999). This nuclear body is distinct from the promyelocytic leukemia body (PML-NB), which is a subnuclear structure present in most cell types and tissues (Salomoni and Pandolfi, 2002). PML is a tumor suppressor inactivated in acute promyelocytic leukemia (APL) and the essential component of the PML-NB (Salomoni and Pandolfi, 2002). In addition to PML, the APB contains telomeric DNA, DNA repair proteins such as MRE11, NBS1 and Rad50, RPA, Rad52, and the telomere repeat binding factors TRF1 and TRF2 (Yeager et al., 1999; Wu et al., 2000, 2003; Zhu et al., 2000; Naka et al., 2002).

TRF2 is a sequence-specific DNA binding protein that binds the duplex array of TTAGGG repeats at human telomeres. It has been shown to protect telomeres from end-to-end fusions through the formation of the t-loop (de Lange, 2002). The overexpression of TRF2 causes telomere attrition in vitro and in vivo (Karlseder et al., 2002; Blanco et al., 2007). Evidence has recently emerged suggesting a role for TRF2 as an oncogene in the absence of telomerase. Overexpression of TRF2 in the skin of telomerase-deficient mice accelerates carcinogenesis and increases telomere recombination, implying that TRF2 is oncogenic and favors the activation of ALT (Blanco et al., 2007). In this respect, TRF2 was found overexpressed in hepatocellular carcinoma (Oh et al., 2005). Furthermore, TRF2 has been shown to delay the onset of senescence by protecting critically short telomeres from fusion and repressing chromosome end-to-end fusions in presenescent cultures (Karlseder et al., 2002). Uncapped telomeres resemble double-strand breaks and it is the presence of the telomere capping complex, named shelterin (de Lange, 2005), that circumvents the activation of a DNA damage response. Removal of TRF2 results in the localization of active ATM to the unprotected telomeres (Takai et al., 2003), eventually inducing ATM-dependent apoptosis in telomerase-positive tumor cell lines or

Correspondence to Paolo Salomoni: ps90@le.ac.uk

Abbreviations used in this paper: ALT, alternative lengthening of telomere; APB, ALT-associated PML body; APL, acute promyelocytic leukemia; DOX, doxycycline; HR, homologous recombination; NB, nuclear body; NHEJ, non-homologous end joining mechanism; PML, promyelocytic leukemia.

The online version of this paper contains supplemental material.

The Journal of Cell Biology, Vol. 179, No. 5, December 3, 2007 855–867
http://www.jcb.org/cgi/doi/10.1083/jcb.200703020

irreversible cell cycle arrest in primary cells (Karlseder et al., 1999, 2002). TRF2 has been shown to interact with ATM, through S1981 in an unphosphorylated state, and block its activation (Karlseder et al., 2004). Interestingly, ATM is involved in telomere maintenance in flies, which lack telomerase and maintain their telomeres through transposition, thus suggesting that also in vertebrates ATM's role may not be limited to inducing a DNA damage response (Bi et al., 2005). Remarkably, recent studies demonstrate that indeed ATM is important in regulating the telomere end structure after replication and ATM inhibition results in telomere end-to-end fusions (Verdun et al., 2005; Verdun and Karlseder, 2006). Nevertheless, it is currently unclear whether ATM has a role in ALT.

The tumor suppressor p53 is a downstream target of ATM and is required for the induction of apoptosis and senescence upon TRF2 down-regulation. It has been proposed that p53 specifically inhibits DNA synthesis and delays exit from S phase in ALT cells by interfering with telomeric recombination (Razak et al., 2004). PML is a known modulator of p53 and regulates its function at multiple levels: (i) it induces p53 accumulation into PML-NBs upon stress, thus causing p53 acetylation and transcriptional activation (Pearson et al., 2000); and (ii) it sequesters Mdm2 to the nucleolus, thus indirectly inhibiting p53 ubiquitylation and degradation (Bernardi et al., 2004). Vice versa, PML itself is a transcriptional target of p53, thus adding a degree of complexity to the whole picture (de Stanchina et al., 2004). Despite several studies indicating that p53 can associate with PML in the PML-NB, it is still an object of controversy whether p53 localization to PML-NB is required for its activation.

In this study, we set out to determine the effects of alterations to the shelterin complex on ALT cells. To this end, we decided to interfere with the function of the shelterin component TRF2 by multiple approaches. Interestingly, lack of TRF2 leads to loss of telomeric DNA and genomic instability. However, this is not associated with a marked induction of cell death, but rather with decreased growth and induction of cellular senescence. Furthermore, in ALT cells, unlike in telomerase-positive cells, ATM is constitutively active, but it is only upon TRF2 down-regulation or inhibition that the ATM target p53 is phosphorylated and activated. In this context, PML is essential for p53-dependent induction of p21. Overall, our findings provide new insights into the consequences of shelterin alterations in ALT cells.

Results

Effects of TRF2 knockdown in ALT cells

We first set out to determine the effect of TRF2 down-regulation on colony formation of ALT cells. To stably silence TRF2, we constructed expression vectors encoding shRNAs for TRF2 and introduced them in U2OS cells, which are p53-proficient. TRF2 knockdown reproducibly resulted in decreased number of colonies in colony-forming assays (Fig. 1 A). A number of clones derived from isolated colonies displayed a substantial decrease in TRF2 protein levels both by Western blotting and immunofluorescence (Fig. 1 B and Fig. 3 A). As inhibition of TRF2 in telomerase-positive cells lines leads to induction of apoptosis, we analyzed apoptosis levels in TRF2-depleted clones. Only a modest increase in apoptosis was observed in the G10 TRF2 shRNA clone by both subdiploid peak analysis and Hoechst staining (Fig. 1, C and D). We next used a dominant-negative TRF2 mutant, ΔBΔM, which lacks both the Basic and Myb domain and sequesters endogenous TRF2 away from telomere ends (van Steensel et al., 1998). We generated U2OS clones stably expressing ΔBΔM (Fig. S1 A, available at http://www.jcb.org/cgi.content/full/jcb.200703020/DC1) and analyzed levels of spontaneous apoptosis by Hoechst staining. A marginal increase in apoptotic cells was detected only in one of the two ΔBΔM clones (G3), thus suggesting that ALT cells can escape some of the consequences of TRF2 inactivation (Fig. 1 E). To confirm the growth-suppressive effect of TRF2 silencing in a more controlled system, we generated inducible clones expressing shRNAs against TRF2 under the control of doxycycline (DOX). Western blotting and immunofluorescence analyses demonstrated that expression of TRF2 was completely shut down 72 h after the addition of DOX (Fig. 1 F). Importantly, formation of colonies was clearly decreased in the presence of DOX, thus confirming data obtained using the stable TRF2 knockdown (Fig. 1, A and G).

As lack of substantial cell death induction in TRF2-depleted cells could be the result of selection of resistant clones through compensatory mechanisms acting on the apoptosis machinery, we set to determine the immediate effects of TRF2 depletion/inactivation in transient expression experiments. TRF2 was knocked down using RNAi oligonucleotides in U2OS cells (Fig. S1 B). Strikingly, transient TRF2 silencing had no effect whatsoever on cell death up to 72 h (Fig. S1 C). Furthermore, apoptosis was not induced upon DOX treatment in inducible clones up to 72 h (unpublished data). Finally, transient expression of ΔBΔM (Fig. S1 D, left) did not lead to induction of cell death compared with empty vector-transfected cells (Fig. S1 D, right). Similar results were obtained using the p53-deficient ALT cell line SAOS2 (Fig. S3 D, available at http://www.jcb.org/cgi.content/full/jcb.200703020/DC1; and unpublished data). In contrast, ΔBΔM induced cell death in HeLa in transient, and we were unable to obtain stable clones (unpublished data).

In telomerase-positive cells, lack of TRF2 at telomeres induces end-to-end fusions, which is the result of the de-inhibition of the nonhomologous end joining mechanism (NHEJ). To test whether end-to-end fusions could be induced in ALT cells, we stained metaphases from ΔBΔM-transfected U2OS cells with a telomeric PNA probe to visualize telomeres. Cytogenetic analysis of U2OS metaphases from sorted cells transiently expressing the ΔBΔM allele showed ∼16% (13/81 cells) contained long chains of fused chromosomes with multiple internal telomere signals and ring chromosomes (Fig. S1 E). This indicates that transient expression of the ΔBΔM allele causes chromosome fusion via NHEJ in a minority of U2OS ALT+ cells in contrast to the high frequency of fusions seen in telomerase + cells (van Steensel et al., 1998). The decreased proportion of metaphases displaying end-to-end fusions may explain why ALT cells appear to cope better following TRF2 down-regulation or inactivation. For instance, following clonal selection and expansion none of the G10 TRF2-depleted or control cells (pRS26) contained long chains of telomere-telomere fused chromosomes (0/25 cells for each cell line; unpublished data).

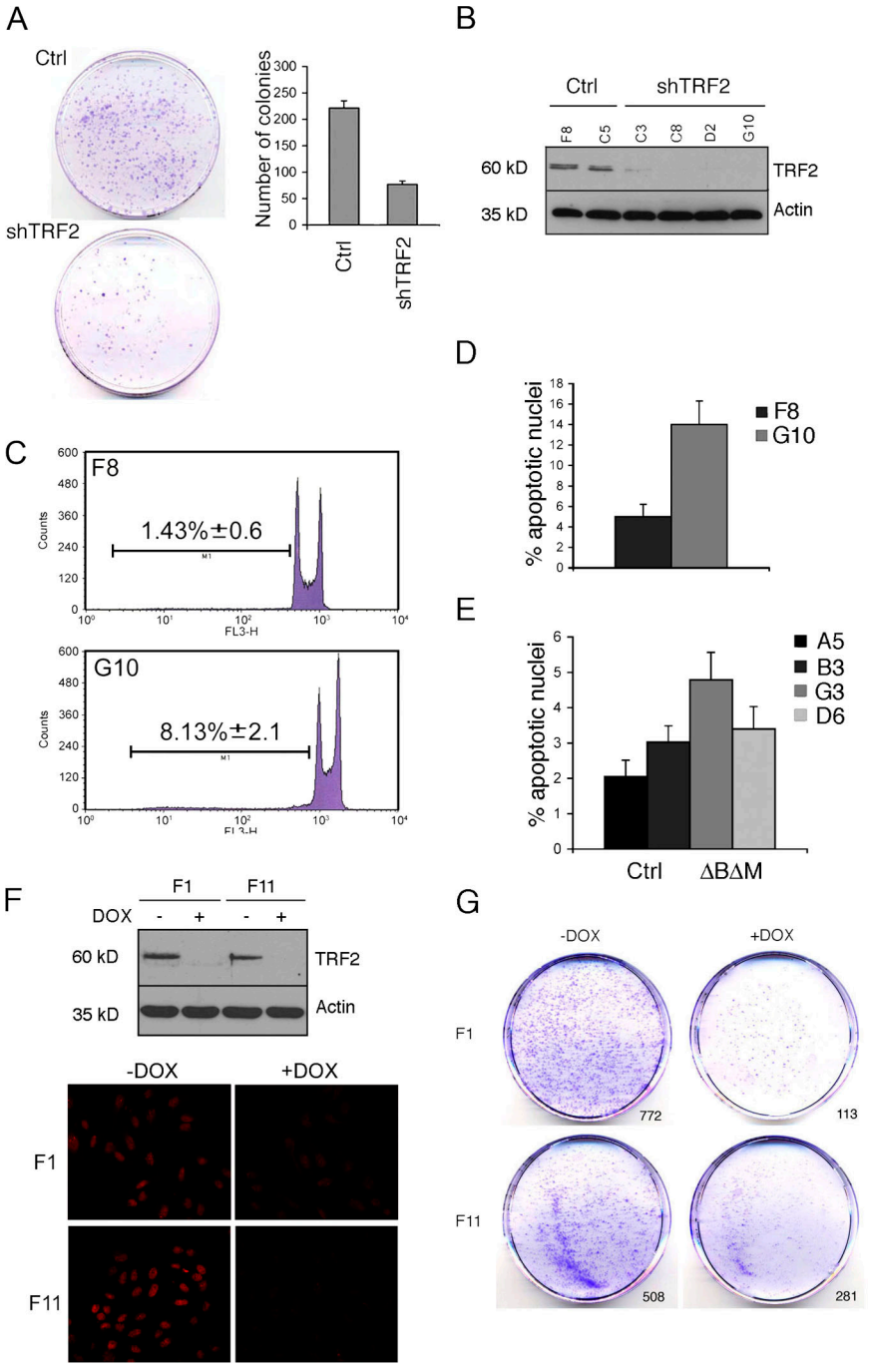

Figure 1. **Effects of PML and TRF2 stable down-regulation.** (A) TRF2 knockdown suppresses colony formation. U2OS cells were transfected with empty pRETROsuper (Ctrl) or with pRS shRNA expression vectors targeting TRF2 (shTRF2) and selected for 10 d. Cells were stained using crystal violet, and colonies were counted. Representative pictures are shown. Graph represents means of three experiments ± standard deviations. (B) Colonies from pRS and TRF2-pRS-transfected cells were picked and analyzed by SDS-PAGE using anti-TRF2 and anti-Actin antibodies. Control clones are indicated. (C) Modest induction of apoptosis in stable TRF2-depleted clones. F8 and G10 cells were stained with propidium iodide and analyzed using a cytometer. Subdiploid peaks are indicated. Histograms are representative of three independent experiments, while values represent means of experiments ± standard errors. (D) Hoechst staining of live cells shows increased apoptotic nuclei in G10 cells. Histograms are representative of three independent experiments, while values represent means of experiments ± standard errors. (E) Hoechst staining of live cells shows increased apoptotic nuclei in ΔBΔM-expressing clones. Histograms are representative of three independent experiments, while values represent means of experiments ± standard errors. (F) TetON inducible U2OS clones F1 and F11 lose TRF2 expression following doxycycline (DOX) induction (three days). SDS-PAGE was blotted with anti-TRF2 and anti-Actin antibodies (top). Induced and un-induced cells were also stained for immunofluorescence using anti-TRF2 antibodies (bottom). (G) Colony formation is impaired in inducible cells cultured in the presence of doxycycline. The same number of cells from F1 and F11 clones were plated and cultured in the presence of DOX for two weeks. Number of colonies is shown. Representative of two independent experiments with similar results.

Despite the substantial lack of end-to-end fusions, TRF2-depleted U2OS cells displayed features of genomic instability. First, several mitotic figures in TRF2-depleted cells were abnormal (51/119 in G10 cells versus 20/218 in control cells), as several anaphase bridges and lagging chromosomes were clearly detected (Fig. S2 A, available at http://www.jcb.org/cgi.content/full/jcb.200703020/DC1). This was accompanied by increased nuclear size and/or aberrant morphology detected in more than 60% of TRF2-depleted cells. In addition to this, we found a proportion of polynucleated cells in cultures of TRF2-depleted cells (11%), and a small number (1–2%) of tripolar mitoses were also present (Fig. S2, A and B). Aberrant nuclear morphology was also detected in ΔBΔM-expressing cells in transient, in ΔBΔM-expressing clones and in mixed populations (Fig. S2 C). We also detected numerous micronuclei in TRF2-depleted cells, which can be the result of either lagging chromosomes or supernumerary centrosomes (G10 clone; Fig. S2 B) (Brinkley, 2001; Kirsch-Volders et al., 2002). Indeed, supernumerary centrosomes were found in TRF2-depleted cells, thus suggesting the presence of centrosomal dysfunction (unpublished data).

Interestingly, TRF2-depleted cells appeared larger than control cells (Fig. S2 D). This prompted us to run TRF2-deficient cells through a CASY counter and a cytometer. A clear increase in cell size was demonstrated in independent TRF2-deficient

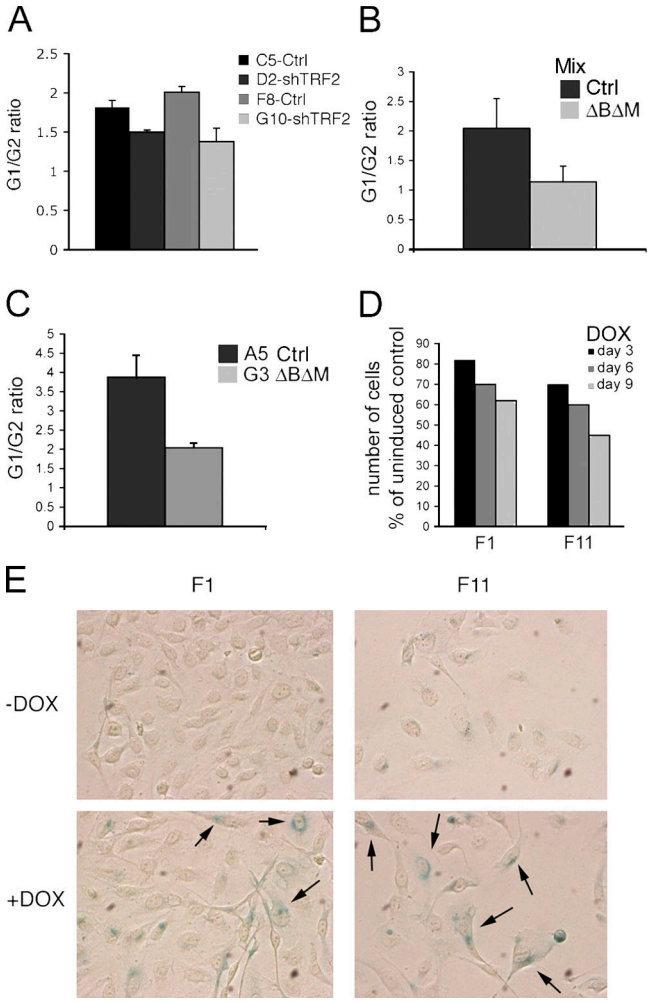

Figure 2. **Cell cycle alterations and cellular senescence in cells lacking TRF2.** (A) TRF2-depleted U2OS clones display increased accumulation in the G2 phase of cell cycle. Fixed control and TRF2 depleted clones were stained with propidium iodide (PI) and analyzed for cell cycle profiles. Data shown are means of three independent experiments ± SEM. (B) ΔBΔM-expressing mix populations show increased accumulation in the G2 phase. U2OS cells were transfected with GFP and control or ΔBΔM vectors and sorted. Cells were analyzed for cell cycle distribution using PI. Data shown are means of three independent experiments ± SEM. (C) ΔBΔM-expressing clones accumulate in the G2 phase. ΔBΔM-expressing clones were analyzed for cell cycle profiles using PI staining. Data shown are means of three independent experiments ± SEM. (D) Inducible TRF2 depletion results in decreased proliferation. Inducible shRNA clones were treated with doxycycline or left untreated, and cells were counted at different passages from stimulation. Data are representative of two independent experiments with similar results and are expressed as percentage of un-induced control. (E) Induction of cellular senescence upon TRF2 knockdown. Inducible clones F1 (left two panels) and F11 (right two panels) were cultured in the absence or presence of Doxycycline for 7 d and stained for SA-βGal. Images were acquired by light microscopy.

clones compared with control ones (Fig. S2 E). Furthermore, DOX-dependent down-regulation of TRF2 in inducible clones also resulted in increased cell size at all time points analyzed (Fig. S2 F).

As induction of cell death is very likely not a major contributor of the observed decrease in colony formation, diminished proliferation is the most plausible explanation. To test this, we analyzed cell cycle profiles in TRF2-depleted cells and found an increase in the proportion of cells in the G2 phase of cell cycle (Fig. 2 A). Mixed populations of sorted cells expressing the ΔBΔM mutant also displayed an accumulation in the G2 phase (Fig. 2 B), and similar changes were observed in ΔBΔM-expressing clones (Fig. 2 C). Finally, we studied proliferation in inducible clones and found that the number of TRF2-depleted cells compared with control uninduced cells progressively decreases following addition of DOX (Fig. 2 D). Increased cell size and diminished proliferation are two of the features of cellular senescence. Indeed, upon DOX treatment inducible clones became strongly positive for acidic βgal (SA-βgal), a marker of cellular senescence (Fig. 2 E).

APB status in TRF2-depleted cells

As TRF2 is one of the constituents of APBs, we set to investigate whether TRF2 depletion/inactivation has an effect on APB formation. Stable TRF2 down-regulation did not affect PML localization and the colocalization between TRF1 and MRE11, which constitutes a marker for APBs (Fig. 3 A and unpublished data). Importantly, colocalization between PML, TRF1 and telomeric DNA was also not affected (Fig. 3 B). Nevertheless, a decrease in the overall number of APBs was observed, which however correlates with a reduction in the intensity of telomeric foci in each nucleus (Fig. 3, C and D). To determine whether the observed effects on telomeric signals could be applied also to other ALT cells, we generated TRF2-depleted clones of the ALT cell line SUSM1 (Fig. S3 A, top set of panels). Indeed, the intensity of telomeric signal was reduced also in TRF2-depleted SUSM1 clones (Fig. S3 A, bottom set of panels). In contrast, TRF2 transient down-regulation in U2OS cells did not have an effect on the overall number of APBs, as measured by presence of MRE11/TRF1 and MRE11/PML foci (Fig. S3, B and C; and unpublished data). Finally, another ALT cell line, SAOS2, was used to confirm the effect of TRF2 depletion on APBs. Also in this case, MRE11 localization was not affected by transient TRF2 silencing (Fig. S3 D). Next, we extended our analysis to ΔBΔM-expressing cells in both transient and stable settings. Transient expression of Myc-tagged ΔBΔM (Fig. 3 E) had no effect on the colocalization between telomeric DNA (PNA staining) and PML and the percentage of cells displaying colocalization (Fig. 3 E and unpublished data). We next studied PML/PNA colocalization in stable ΔBΔM clones. As seen in TRF2-depleted U2OS cells, in stable ΔBΔM clones the intensity of PNA foci appeared to be decreased compared with cells transfected with an empty vector (Fig. 3 F). By performing 3D reconstruction of confocal images, we also found that the number of telomeric foci was diminished (Fig. 3 F). APBs were present in ΔBΔM clones, albeit at a reduced number (Fig. 3 F and unpublished data). It is worth noting that the overall proportion of foci containing both PML and telomeric DNA in each given cell did not change, thus suggesting that the reduction in the number of APBs is probably caused by a decrease in the number of foci containing telomeric DNA (unpublished data).

TRF2 down-regulation affects telomere length in ALT cells

One of the possible explanations for the decreased intensity and smaller number of PNA foci in cells lacking TRF2 is that

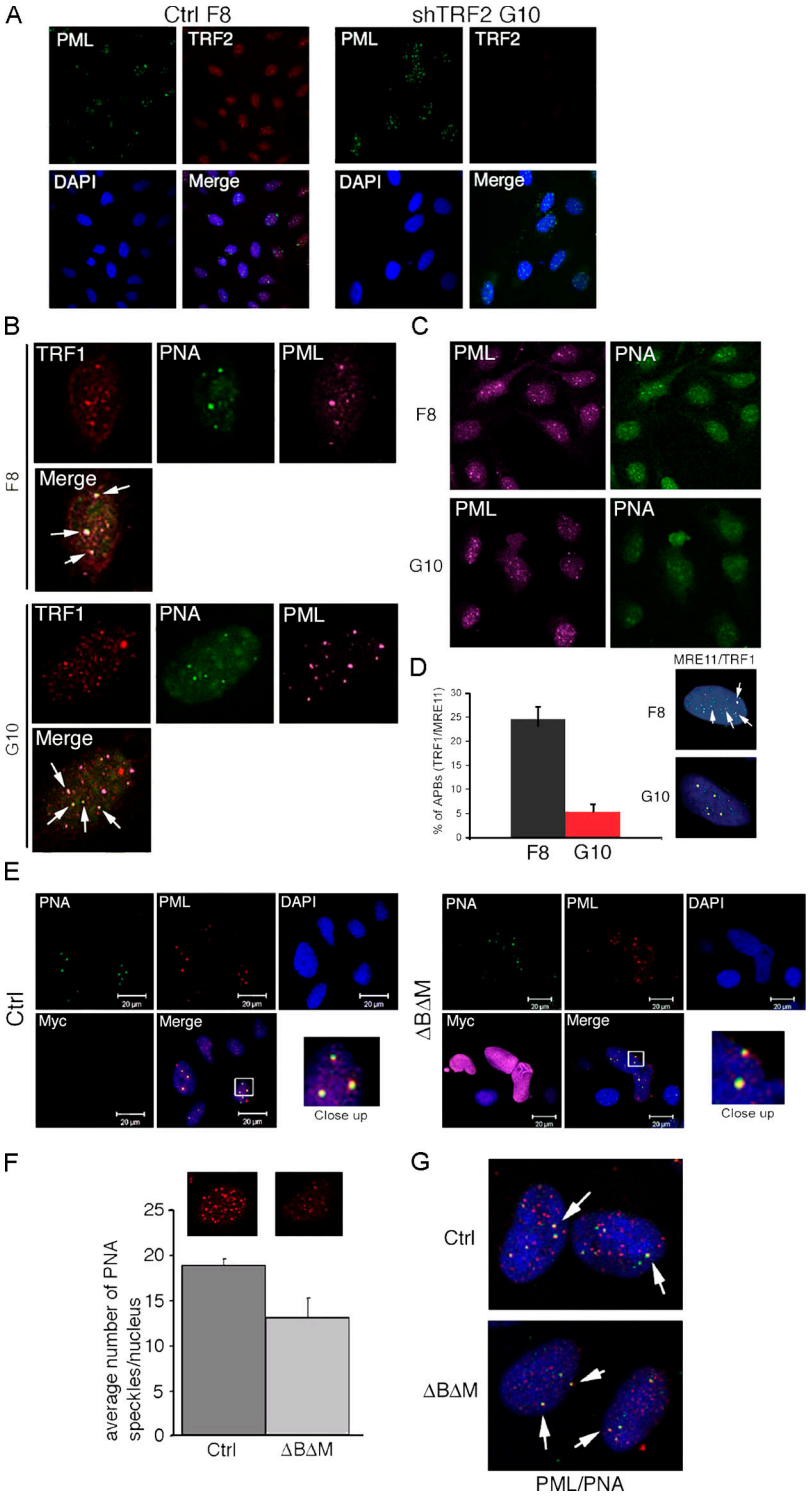

Figure 3. **Effect of TRF2 knockdown or inactivation on APBs.** (A) PML speckled distribution is not affected by TRF2 inactivation in U2OS clones. F8 (Ctrl) and G10 (sh-TRF2) clones were stained with anti-TRF2 and anti-PML antibodies and counterstained with DAPI. (B) TRF1 and PML accumulate at telomeric foci (PNA) in TRF2-depleted cells. Cells were stained with anti-PML and anti-TRF1 antibodies and postfixed. Then, coverslips were dehydrated and processed for FISH. (C) Telomeric signal is decreased in TRF2-depleted cells and number of PML/PNA/PML foci is also reduced. Cells were processed as in B. (D) Percentage of MRE11/TRF1 foci is also decreased in TRF2-depleted cells. Insets show F8 and G10 cells stained with anti-TRF1 (green) and anti-MRE11 antibodies (red; merge signals). DAPI was used to label nuclei. Arrows indicate TRF1/MRE11 positive speckles. Data shown are means of three independent experiments ± SEM. (E) Transient expression of the ΔBΔM TRF2 mutant does not affect PML/PNA co-localization in transient. U2OS cells were transfected with an expression vector encoding Myc-tagged ΔBΔM TRF2 (ΔBΔM) or a control vector (Ctrl) and stained with anti-Myc-tag and PML antibodies. Cells were then post-fixed and processed for FISH. DAPI was used to stain nuclei. (F) Number of telomeric foci is reduced in ΔBΔM-expressing stable clones. Control vector and ΔBΔM TRF2 clones were hybridized with a PNA telomeric probe and analyzed by confocal microscopy. Then, images were 3D-reconstructed. Approximately 100 cells each field were analyzed. Data shown are means of three independent experiments ± SEM. (G) APBs are present in ΔBΔM-expressing clones. Control (Ctrl) and ΔBΔM clones were stained with anti-PML antibodies, post-fixed and processed for FISH as in B.

telomeres are affected. To test this, we analyzed telomere length by pulse-field gel analysis of digested genomic DNA followed by Southern blot hybridization using a telomere-specific probe. We conducted our analysis on empty vector-transfected clones (pRS25, pRS26), shTRF2-expressing clones that did not show TRF2 down-regulation (C5, F8) and on TRF2-depleted clones (G10, C3, D2, C8). Surprisingly, TRF2-depleted U2OS clones displayed shorter telomeres and decreased telomeric signal (Fig. 4 A). Quantitative analysis of the telomere length using the Telometric software confirmed that telomeres are indeed shorter in cells lacking TRF2 (Fig. 4 A, bottom). We extended our analysis to a different passage for clones F8, G10, C3 and C8 (additional population doublings: F8+5.22pd; C3+4.34pd; D2+4.46; G10+4.2) and obtained similar results (unpublished data). This may indicate that the number of population doublings between two time points was insufficient to detect progressive shortening of telomeres.

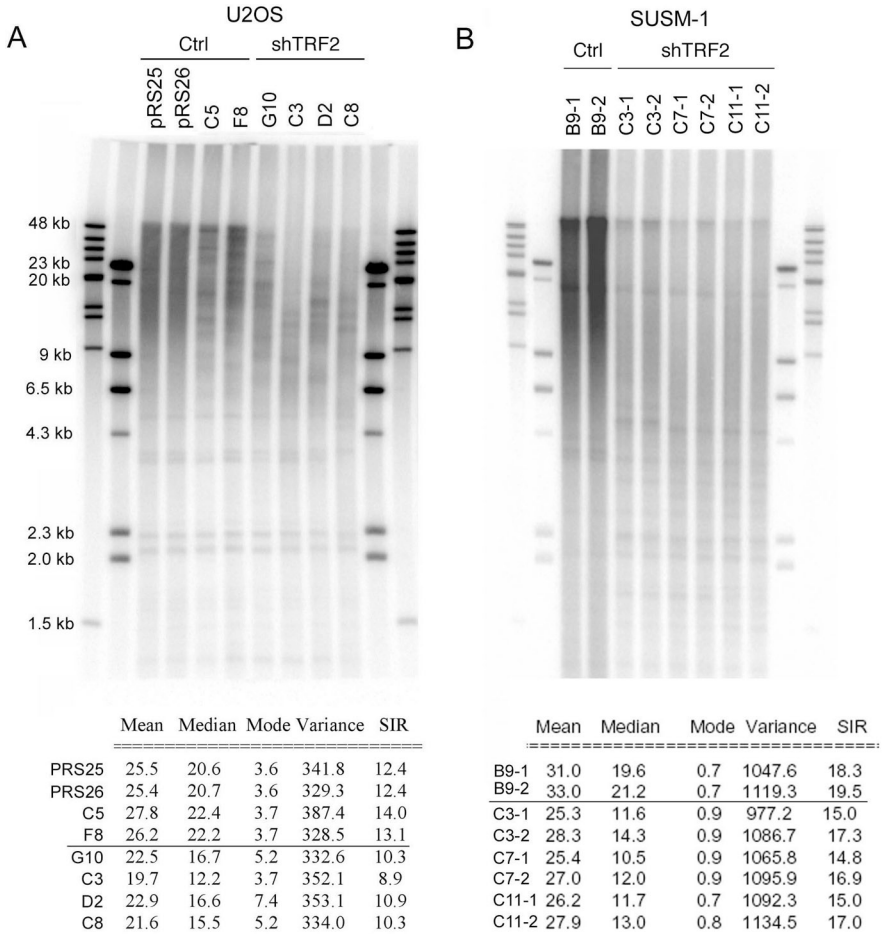

	Mean	Median	Mode	Variance	SIR
PRS25	25.5	20.6	3.6	341.8	12.4
PRS26	25.4	20.7	3.6	329.3	12.4
C5	27.8	22.4	3.7	387.4	14.0
F8	26.2	22.2	3.7	328.5	13.1
G10	22.5	16.7	5.2	332.6	10.3
C3	19.7	12.2	3.7	352.1	8.9
D2	22.9	16.6	7.4	353.1	10.9
C8	21.6	15.5	5.2	334.0	10.3

	Mean	Median	Mode	Variance	SIR
B9-1	31.0	19.6	0.7	1047.6	18.3
B9-2	33.0	21.2	0.7	1119.3	19.5
C3-1	25.3	11.6	0.9	977.2	15.0
C3-2	28.3	14.3	0.9	1086.7	17.3
C7-1	25.4	10.5	0.9	1065.8	14.8
C7-2	27.0	12.0	0.9	1095.9	16.9
C11-1	26.2	11.7	0.7	1092.3	15.0
C11-2	27.9	13.0	0.8	1134.5	17.0

Figure 4. **Shortening of telomeres in TRF2-depleted ALT cells.** (A) TRF2-depleted U2OS clones display shorter telomeres and decreased telomeric DNA hybridization. DNA from empty vector (pRS25, pRS26), TRF2-depleted clones (G10, C3, D2, C8) and clones expressing TRF2 shRNA but not displaying down-regulation (C5, F8) were digested and size separated by PFGE. The resulting Southern blots were hybridized to a telomere specific probe and telomere length was measured using the Telometric software (bottom table). (B) In TRF2-depleted SUSM-1 clones (C3, C7, C11) compared with a empty vector clone (B9) telomere length is also reduced and there is a substantial reduction in telomeric DNA signal. Two different passages are shown (additional 2.5 population doublings). DNAs were processed as in A. Bottom table shows Telometric analysis of telomere length.

In this respect, the fact that TRF2-depleted clones tend to lose silencing through time did not allow us to calculate the shortening rate. Moreover, we found that stable TRF2 depletion in a different ALT cell line, SUSM1, led to telomere shortening, albeit to a lesser extent, and to a markedly decreased total hybridization signal, thus demonstrating that the loss of telomeric DNA is not limited to a single ALT cell line (Control clone B9, TRF2-depleted clones C3, C7 and C11; Fig. 4 B). The decreased intensity of the signal in TRF2-depleted cells is not due to uneven loading, as demonstrated by using a probe for the minisatellite MS1 (Fig. S4, A and B; available at http://www.jcb.org/cgi.content/full/jcb.200703020/DC1). Loss of telomeric DNA was confirmed in U2OS and SUSM1 clones using FlowFISH (Fig. S4 C). To our knowledge, this is first report describing an effect of TRF2 knockdown on telomeric DNA in ALT cells.

ATM status in ALT cells

Inactivation of TRF2 in telomerase-positive tumor cells or primary fibroblasts causes the uncapping of telomeres, which are then recognized as DNA damage sites. This in turn results in ATM activation and induction of p53-dependent cell death or cellular senescence depending on the cell type and transformation status (Bartkova et al., 2006; Di Micco et al., 2006; Mallette et al., 2007). We reasoned that TRF2 down-regulation in ALT cells could have a similar effect. To this end, we analyzed ATM activation by using an antibody recognizing phosphorylated serine 1981, which is an accepted activation marker. Surprisingly, we observed that phosphorylated ATM (P-ATM) is present in 100% of control and TRF2-depleted cells and accumulates in nuclear speckles (Fig. 5 A). Approximately 10 ATM speckles were found in each nucleus of parental or empty vector-transfected U2OS (Fig. 5 C and unpublished data). To demonstrate that the staining was specific, we treated U2OS cells with caffeine, which is an inhibitor of ATM and ATR. The P-ATM signal was indeed almost completely abolished in cells cultured with 10 mM caffeine for 45 min (unpublished data). We next analyzed whether P-ATM colocalized with PML and telomeric foci. Remarkably, ~25% of cells displayed ATM/PML colocalization and in each cell half of P-ATM speckles coincided with PML (Fig. 5, B and C; 52 ± 8.65% and unpublished data). P-ATM also colocalized with PNA (and PML) in U2OS cells (Fig. 5, B and C), and nearly 40% of P-ATM foci contained PNA in U2OS and SAOS2 cells (Fig. 5, B, C, and E and unpublished data). In addition, colocalization between P-ATM, PNA and TRF2 was demonstrated in both U2OS and SAOS2 cells (Fig. 5, E and F). Finally, PNA/PML colocalization was also detected in SUSM1 cells (Fig. S5 A, available at http://www.jcb.org/cgi.content/full/jcb.200703020/DC1). However, a percentage of P-ATM speckles were negative for either PML or TRF2, thus suggesting that P-ATM can also localize to nuclear domains or sites of DNA damage other than APBs in ALT cells. To determine whether ATM

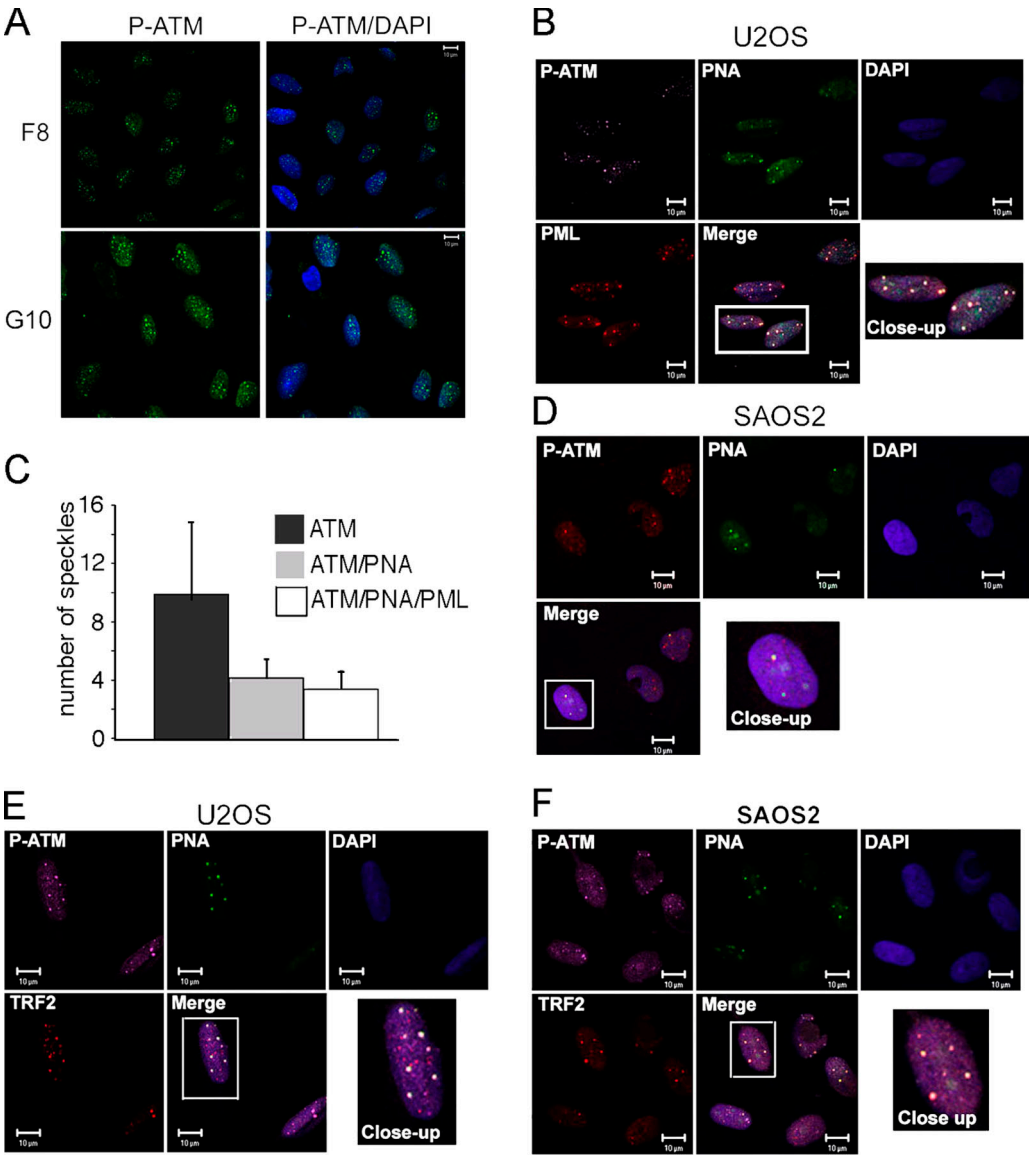

Figure 5. **ATM is phosphorylated and localizes at APBs in ALT cells.** (A) ATM is phosphorylated at serine 1981 in control U2OS cells and TRF2-depleted cells. F8 and G10 clones were stained using an anti-S1981 ATM antibody (P-ATM). Nuclei were stained using DAPI. Figures shown are representative of three independent experiments. (B) P-ATM accumulates at PML-positive telomeric foci (APBs) in U2OS cells. Cells were stained with anti-PML antibody and post-fixed. Cells were then dehydrated and process for FISH using a FITC-conjugated PNA probe. DAPI was used to visualize nuclei. (C) Most ATM/PNA speckles are positive for PML. Graph shows number of P-ATM, P-ATM/PNA, P-ATM/PNA/PML speckles each nucleus. (D) P-ATM colocalizes with PML and telomeric foci also in SAOS2 cells. Cells were processed as in (B). (E) (F) PNA/P-ATM speckles are also positive for TRF2 in U2OS (E) and SAOS2 (F). Cells were stained with anti-P-ATM, anti-TRF2 antibodies and then post-fixed. Coverslips were processed for FISH using a FITC-labeled PNA probe. DAPI was used to visualize nuclei.

targets were phosphorylated in ALT cells, we stained U2OS with an antibody directed against phosphorylated ATM/ATR targets and found that all P-ATM speckles are also positive for phosphorylated ATM/ATR targets (Fig. S5 B). We next analyzed the phosphorylation status and localization patterns of the ATM target NBS1 using phospho-specific antibodies. NBS1 was indeed phosphorylated in ALT cells and colocalized with PML and P-ATM in ~23% of cells (Fig. S5 B; unpublished data). In contrast, nuclei of telomerase-positive HeLa and MCF7 did not display ATM/ATR targets-positive speckles (Fig. S5 C; unpublished data). Finally, primary BJ fibroblasts were also negative for P-ATM (Fig. S5 D). In summary, P-ATM is found in ALT cells at steady state, in part accumulates in APBs, and a number of its targets are phosphorylated and partially colocalize with APBs.

Effect TRF2 down-regulation or functional inhibition on p53 activation

As p53 is phosphorylated at serine 15 upon ATM activation, we analyzed p53 phosphorylation status at this residue in ALT cells. We analyzed a panel of ALT and telomerase-positive cell lines and found that p53 was phosphorylated (P-p53) in three different ALT cell lines, VA13, GM847 and JFCF6 (Fig. S5 E). However, similar amounts of P-p53 were also found in the related cell line JFCF6-T, which is telomerase-positive (Fig. S5 E).

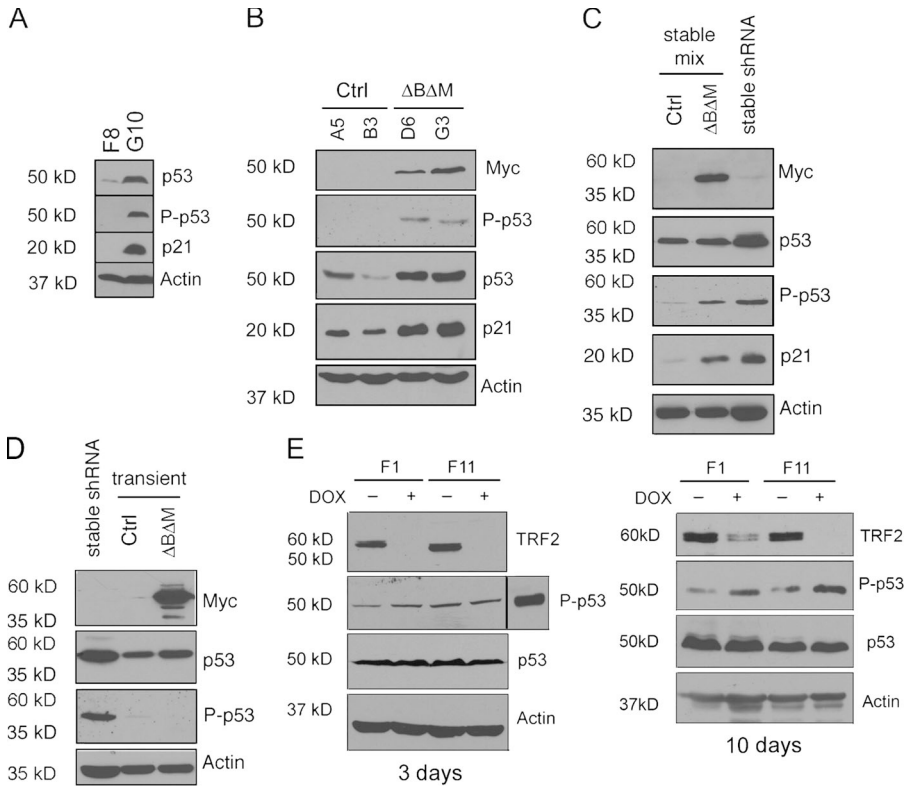

Figure 6. **p53 is activated upon prolonged TRF2 down-regulation or inactivation.** (A) p53 is phosphorylated and p21 induced in a TRF2-depleted clone. Control (F8) and TRF2-depleted (G10) clones were stained with anti-p53, anti-phosphor serine 15 p53 (P-p53), anti-p21 and anti-Actin antibodies. Data are representative of two independent experiments with similar results. (B) p53 is activated in ΔBΔM-expressing U2OS clones. Extracts from empty vector (A5, B3) and ΔBΔM-expressing (G3, D6) clones were probed as in (A). Data are representative of two independent experiments with similar results. (C) p53 is activated also in mix populations from control vector- and ΔBΔM-transfected U2OS cells. Extracts were analyzed as in (A) and (B). (D) Transient inactivation of TRF2 does not lead to p53 activation. U2OS cells were transfected with control or ΔBΔM vectors, and with GFP. Cells were then sorted, cultured for 10 d and then selected for additional five days. p53 activation was studied as in (B), (C). (E) Effects of short-term (left) or long-term (right) TRF2 down-regulation using a doxycycline (DOX)-inducible system. Inset in left panel shows p53 phosphorylation in shTRF2 stable clone. Two independent inducible clones (F1, F11) were treated with DOX for 3 (left) or 10 d (right) and analyzed for p53 activation as in (D).

VA13, JFCF6 and JFCF6-T have been immortalized using SV40 T antigen, thus suggesting that the presence of high p53 levels is due to the immortalization process or the presence of T antigen per se. In contrast, p53 was not phosphorylated in the remaining telomerase-positive and ALT cell lines (Fig. S5 E). We focused on U2OS cells, which are the only available p53-proficient ALT cell lines not expressing SV40 T antigens. As mentioned above, p53 is not phosphorylated in control U2OS cells (F8; Fig. 6 A). However, in TRF2-depleted cells (G10) p53 is phosphorylated and its levels increased (Fig. 6 A). This was accompanied by the induction of the p53 target gene and cell cycle inhibitor p21 (Fig. 6 A). p21 expression is dependent on p53 in osteosarcoma cells, while in p53-deficient SAOS2 cells p21 is expressed at very low levels and does not respond to genotoxic stress (unpublished data). In contrast, p53 proapoptotic targets, such Bax and Puma were not affected (unpublished data). We then analyzed p53 status in U2OS clones expressing ΔBΔM and found that p53 was induced at protein levels and was phosphorylated at serine 15 (Fig. 6 B). Furthermore, p21 was augmented in ΔBΔM cells (Fig. 6 B). To exclude an effect due to clonal selection, we transfected U2OS cells with either a ΔBΔM expressing vector or control vector in conjunction with GFP. Cells were sorted, selected and analyzed after two weeks for p53 activation. Indeed, p53 was phosphorylated and p21 increased in ΔBΔM expressing cells, while p53 levels were not affected (Fig. 6 C).

As apoptosis is not induced in cells ΔBΔM-transfected U2OS cells in transient, we studied whether p53 was activated in these settings. U2OS were cotransfected with ΔBΔM or control plasmid and GFP, and sorted. In sorted ΔBΔM-expressing cells p53 phosphorylation was not induced and p21 levels were unchanged (Fig. 6 D). To substantiate these findings in a more controlled system, we followed p53 phosphorylation in shRNA inducible clones. Similar to what was seen in transient transfection experiments, p53 phosphorylation was not increased early on after induction despite the complete down-regulation of TRF2 (three days; Fig. 6 E, left). In contrast, P-p53 levels were augmented at 10 d, and p21 was also induced (Fig. 6 E, right; unpublished data), thus suggesting that in ALT cells p53 activation is not an immediate consequence of TRF2 down-regulation or inactivation.

We next analyzed the localization of p53 in U2OS cells, and found that more than 20% of cells displayed p53 in nuclear speckles, which were also positive for PML, TRF1, TRF2 and telomeric DNA (Fig. 7 A and Fig. S5 F). In contrast, p53 localization to APBs was diminished upon TRF2 silencing (Fig. S5 G). Also in ΔBΔM clones p53 accumulation in APBs was decreased following TRF2 depletion (Fig. S5 H). This is very likely due to the reduced number of APBs and of foci containing telomeric DNA we have observed in stable clones lacking TRF2. p53 failed to colocalize with TRF1, TRF2 and PML in telomerase-positive MCF-7 and HeLa (unpublished data). Interestingly, in SUSM-1 p53 is mutated and still accumulates at APBs (unpublished data) (Mihara et al., 1996), thus indicating that p53 mutation status does not influence its localization to APBs. Because TRF2 appears to colocalize with p53, we tested whether it interacts with p53 by coimmunoprecipitation. While p53 was readily detected in anti-PML immunoprecipitates (IP), TRF2 was not found in anti-p53 IP, and, vice versa, p53 was not detected in anti-TRF2 IPs (Fig. S5 I). This suggests that TRF2, at least in these experimental conditions, does not interact with p53 directly.

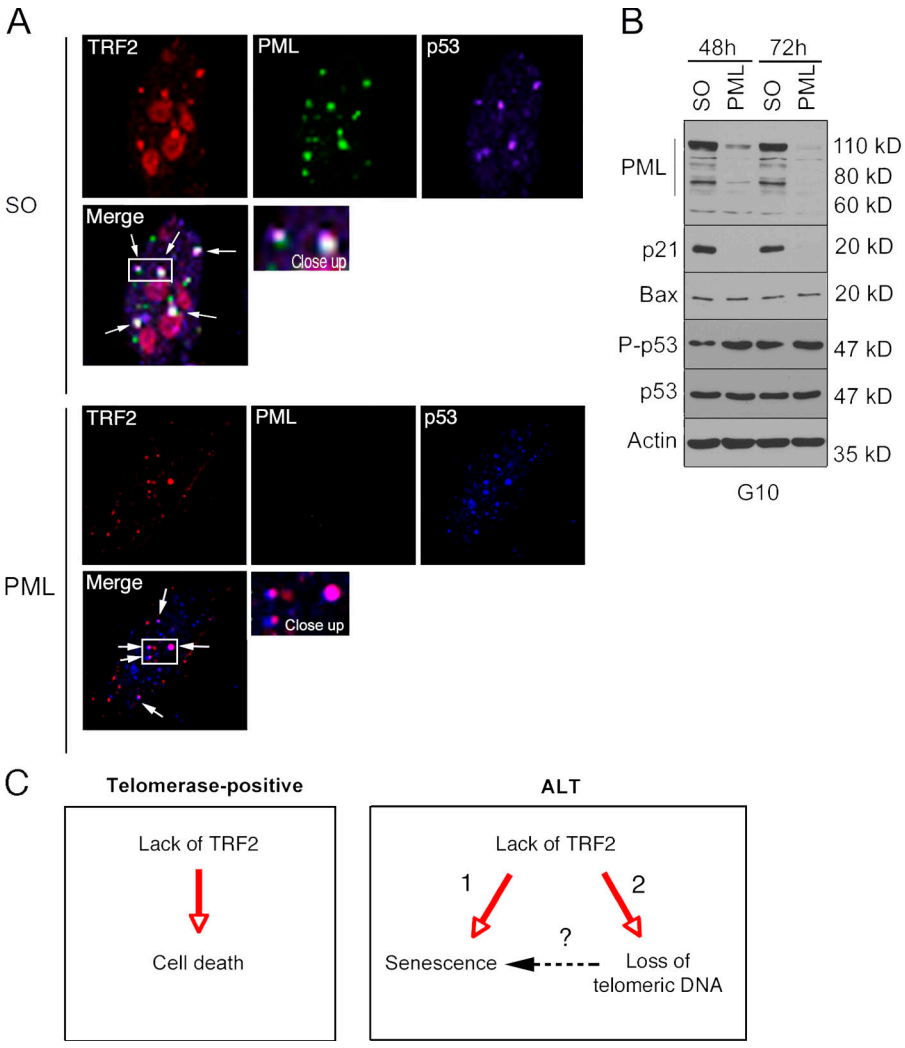

Figure 7. **p53 activation upon TRF2 silencing relies on PML.** (A) PML does not affect p53 localization to TRF2-containing speckles. U2OS cells were electroporated with RNAi oligos against nuclear PML isoforms (PML) or control scrambled oligos (SO) and stained with anti-TRF2, anti-p53 and anti-PML antibodies. (B) PML silencing abrogates p21 induction in TRF2-depleted U2OS cells. The TRF2-depleted G10 clone was electroporated with PML RNAi oligos and analyzed for expression of PML, p21, Bax, P-p53, p53 and Actin using relevant antibodies. Data representative of two independent experiments with similar results. (C) Proposed model for TRF2 function in ALT cells. In telomerase positive cells TRF2 inactivation results in the immediate activation of the ATM/p53 axis for induction of cell death. In contrast, in ALT cells, where ATM is constitutively active, TRF2 inactivation has two major effects: (1) Cellular senescence. (2) Loss of telomeric DNA. It is still unknown whether loss of telomeric DNA could itself trigger cellular senescence.

PML is essential for p53 activation upon TRF2 knockdown

PML has been previously shown to regulate p53 localization to PML-NB in primary or telomerase-positive cells (Salomoni and Pandolfi, 2002). However, its role in regulating p53 localization in ALT cells was unknown. To test this, we knocked down PML transiently and analyzed p53 localization. Surprisingly, PML depletion did not affect p53 colocalization with TRF2 and P-ATM, thus indicating that PML does not regulate p53 localization to dysfunctional/recombining telomeres (Fig. 7 A and unpublished data). Steady-state levels of the p53 target gene p21 were not affected by PML down-regulation either (unpublished data), again suggesting that the role of PML lies elsewhere. Then, we set out to determine whether PML regulates p53 function in TRF2-depleted cells. To this end, we transfected scrambled and PML RNAi oligonucleotides into TRF2-depleted G10 cells and analyzed the effect of PML down-regulation on p53 activation. Remarkably, the induction of p21 was completely abolished in PML-depleted G10 cells, thus indicating that PML is indispensable for p53 activation upon TRF2 silencing (Fig. 7 B). In contrast, no effect on p53 phosphorylation or total protein levels was detected, thus suggesting that PML does not interfere with ATM-dependent p53 phosphorylation or p53 stability in this context (Fig. 7 B).

Discussion

The involvement of TRF2 and the shelterin complex in telomere protection and maintenance has been extensively studied in telomerase-positive tumor cell lines. However, the role of TRF2 in ALT cells has not been investigated in depth. For this reason, we used a number of approaches, ranging from RNAi to functional inhibition, to manipulate TRF2 function in ALT cells. Colony formation experiments clearly show that RNAi-mediated TRF2 knockdown results in a marked decrease in the number of colonies, thus implicating an effect on either apoptosis or cell cycle, or both. Nevertheless, we find that apoptosis is not induced in TRF2-depleted cells or in cells expressing the dominant-negative ΔBΔM mutant in transient, and only moderately in stable settings. In a previous study, the ALT cell line SAOS2 was shown to be resistant to the cytotoxic effects of TRF2 inactivation, and this was ascribed to the absence of p53 (Karlseder et al., 1999). However, we show here that U2OS cells, which, unlike SAOS2, possess an intact p53 pathway, are resistant to the apoptotic effect of TRF2 knockdown, indicating that the presence of p53 is not sufficient to cause cell death. Remarkably, p53 is not activated in U2OS cells following transient TRF2 silencing or ΔBΔM-induced inactivation. This is not due to lack of telomere

deprotection, as end-to-end fusions can be induced in U2OS cells lacking TRF2 function (albeit in a small proportion of cells), thus indicating that the nonhomologous end joining (NHEJ) pathway is at least apparently functional. In contrast, long-term TRF2 inactivation or silencing results in p53 activation and induction of its target gene p21. This is accompanied by an accumulation in the G2 phase of cell cycle, reduced proliferation and induction of cellular senescence. Again, cell death is not a major component of the cellular response to TRF2 inactivation. These findings clearly indicate that the ALT cell line U2OS reacts differently to telomerase-positive tumor cells to alterations of the shelterin complex.

TRF2 is a component of the ALT-associated PML body (APB), a marker of ALT cells, which has been associated with telomere recombination and the ALT mechanism. Transient TRF2 silencing or ΔBΔM–dependent inactivation has no detectable effects on localization of other APB components to this structure. This is in partial disagreement with a recent work, which showed that in the absence of TRF2 APBs are disrupted (Jiang et al., 2007). The reasons for this apparent discrepancy could be several. In particular, the abovementioned work used methionine restriction-induced cell cycle arrest to artificially increase the number of APBs. In this respect, it is plausible that this treatment per se could have an impact on either APB formation or ALT. Furthermore, in the Jiang et al. work data were not confirmed using the ΔBΔM mutant. Interestingly, stable TRF2 down-regulation or inactivation is associated with a decrease in the number of APBs, which is however concomitant to a decreased intensity and number of telomeric foci in the nucleus. Interestingly, we have demonstrated that TRF2-depleted U2OS and SUSM1 cells display a loss of telomeric DNA compared with control clones. It is presently unknown whether this is due to a decrease in chromosomal or extrachromosomal telomeric DNA. We cannot exclude the possibility that the 'telomere phenotype' of TRF2-depleted "survivor" clones could be somewhat selected as a pro-survival trait. Nonetheless, some lines of evidence suggest that TRF2 is involved in controlling telomere erosion. For instance, it is known that in addition to inhibiting NHEJ, TRF2 can limit homologous recombination (HR)-induced T-loop deletions, which, if uncontrolled, has been shown to cause dramatic telomere attrition and induction of cellular senescence (Wang et al., 2004). T-loop deletions are increased in ALT cells, but this does not result in induction of cellular senescence (Wang et al., 2004). It could be hypothesized that in ALT cells TRF2 could regulate the balance between T-loop deletions and telomere lengthening, which in turn could represent a checkpoint for induction of senescence. As a result of this, the absence of TRF2 would increase T-loop deletions, thus leading to irreversible growth arrest (Fig. 7 C). Alternatively, TRF2 could be involved in masking T-loop deletions to avoid further downstream signaling events. This is a fascinating hypothesis that needs to be tested in the near future.

A very recent paper has proposed that APBs represent sites for SUMOylation of TRF2 and other shelterin components to allow for telomere recombination (Potts and Yu, 2007). Disruption of SUMOylation of the shelterin complex in ALT cells causes the induction of cellular senescence and telomere shortening, and this is accompanied by the disappearance of APBs. These data suggest a functional link between SUMOylation of shelterin components and telomere maintenance and/or protection from telomere erosion. More generally, they suggest that alterations of the shelterin complex in ALT cells result in telomere attrition, which is what we see in our model system.

Recent studies have shown that concomitant TRF2 overexpression and Tert inactivation in the mouse skin results in telomere attrition (Munoz et al., 2005; Blanco et al., 2007). This is apparently in conflict with our findings. However, in late generation TgTRF2/*Tert*$^{-/-}$ animals ALT is activated and telomeres are elongated, suggesting that TRF2 allows ALT activation when telomeres are critically short or dysfunctional.

TRF2 functional inactivation results in uncapping of telomeres, which are recognized as damaged DNA (van Steensel et al., 1998; Karlseder et al., 1999, 2002). This triggers the activation of the ATM/p53 pathway for cell death induction in tumor cell lines and senescence in primary fibroblasts (Karlseder et al., 1999, 2002). Surprisingly, we found that ATM is constitutively phosphorylated in ALT cells and forms nuclear foci, some of which coincide with APBs. Despite the presence of active ATM, p53 is not activated and neither cell cycle arrest nor apoptosis is induced, thus suggesting that the effects of ATM on downstream DNA damage checkpoints are to a certain degree masked in ALT cells. Therefore, TRF2 would act either directly or indirectly to inhibit the propagation of ATM-triggered signals. Another possibility is that ATM function in ALT cells is not limited to transducing a DNA damage signal. For instance, recent studies have demonstrated that ATM is required for correct telomere replication during S phase in primary fibroblasts, thus revealing an unexpected role of ATM in telomere maintenance (Verdun et al., 2005; Verdun and Karlseder, 2006). We are currently investigating ATM function in ALT cells.

Finally, we have shown that p53 colocalizes with PML at APBs in a number of ALT cell lines but not in telomerase-positive cells. Upon TRF2 silencing, PML is indispensable for p53-dependent p21 induction, while it does not affect p53 protein levels or its phosphorylation. It is therefore plausible that PML could affect other p53 posttranslational modifications that govern its transcriptional activation. It is worth noting that p53 still accumulates at telomeres in PML-depleted cells. This suggests that p53 retains the ability to associate with dysfunctional telomeres in the absence of PML, but this is not sufficient to promote its activation.

In summary, our work indicates that differences exist between ALT cells and telomerase-positive cells in the way they react to disruption of TRF2 function and consequent telomere deprotection: (i) In telomerase-positive cells, TRF2 inhibition results in the activation of ATM and the induction of programmed cell death (Fig. 7 C). In contrast, in ALT cells ATM is constitutively active, and TRF2 inactivation/silencing does not trigger apoptosis but rather causes the induction of cellular senescence (Fig. 7 C). (ii) TRF2 depletion results in loss of telomeric DNA (Fig. 7 C), thus suggesting that it may affect the ALT mechanism. In this respect, the potential effect of HR-based T loop deletion on induction of cellular senescence should be carefully investigated.

Materials and methods

Chemicals

All reagents used were from Sigma unless otherwise stated. Scrambled and TRF2 small interfering RNA oligonucleotides were purchased from Ambion.

Antibodies

Antibodies against PML (rabbit) and P-ATM were from Chemicon. Mouse anti–human PML (PGM3), mouse anti–human p53 (DO-1), goat anti–human PML (N19), rabbit anti-TRF2 (N-20) and rabbit anti-Bax were purchased from Santa Cruz Biotechnology. Antibodies against p21, phospho-ATM/ATR targets and phospho-serine 15 p53 were from Cell Signaling Technology (NEB). The anti-Phospho-Chk2 antibody was a kind gift of Dr. Tina Rich (Glasgow University) and was originally purchased from Upstate Biotechnology. Antibodies against MRE11, TRF1 and phospho-NBS1 were purchased from Abcam. Anti-Actin antibodies were purchased from Sigma-Aldrich. Anti-γ-tubulin was a gift of Dr. Andrew Fry (University of Leicester). HRP-conjugated secondary antibodies were from Amersham Biosciences.

Cell culture

Human primary fibroblasts from newborn foreskin, designated BJ, were purchased from the American Type Culture Collection (ATCC). They were cultured in Dulbecco's modified Eagle's medium (Invitrogen) supplemented with 20% fetal calf serum (Sera Laboratories International), SAOS-2 and U2OS osteosarcoma cell lines purchased from ATCC. These cell lines were maintained in Dulbecco's Modified Eagle's Medium (DME) (GIBCO BRL) supplemented with 10% (vol/vol) heat inactivated fetal bovine serum (FBS). IIICF/A2 spontaneously immortalised cells were grown in RPMI 1640 (GIBCO BRL) supplemented with 20% (vol/vol) heat inactivated FBS, 2mM glutamax (L-glutamine). JFCF6-T.1J/11E (ALT) and JFCF6-T.1J/11C (telomerase positive) were maintained in low glucose DME (GIBCO BRL) supplemented with 15% (vol/vol) heat inactivated FBS. The above three cells lines were a gift from Dr. Roger Reddel (Children's Medical Research Institute, University of Sydney). SUSM-1 and GM847 SV40 were obtained from ATCC. The above mentioned cells were maintained in Modified Eagle's Medium (MEM) supplemented with 15% (vol/vol) heat inactivated FBS, 1% (vol/vol) Non-Essential Amino Acids (NEAA) (GIBCO BRL). HeLa and MCF7 cell lines were obtained from ATCC and grown in DME (GIBCO BRL). Cells were grown in a humidified incubator at 37C and 5% CO2/air. All media was supplemented with 100 U/ml penicillin (GIBCO BRL) and 100 mg/ml streptomycin (GIBCO BRL).

Small interfering RNA transient transfection

RNAi duplexes against PML and TRF2 mRNA were used. The oligo sequences are as follows: CGACAGCCCAGAAGAGGAAtt (PML sense); UUCCUCUUCUGGGCUGUCGtt (PML antisense); *TRF2*: GAGGAUGAACUGUUUCAAGtt (TRF2 sense); CUUGAAACAGUUCAUCCUCtt (TRF2 antisense); GGAGGAGUUCCAGUUUCUG (Exon2 sense); CAGAAACUGGAACUCCUCC (Exon2 antisense). The PML oligo was directed against exon 6 (nuclear localization signal), the Exon2 against exon2 and the TRF2 oligo as described by Xu and Blackburn (Xu and Blackburn, 2004). The oligos were transfected by electroporation using a Bio-Rad X-Cell electroporator. Eight million cells were resuspended in 100 μl OptiMEM serum-free medium (Invitrogen) and transferred into 2 mm electroporation cuvettes (Molecular BioProducts). Cells were electroporated at 160 V using an exponentially decaying pulse. Cell viability was determined following electroporation using the trypan blue exclusion assay.

Stable transfection of shRNAs

U2OS cells were transfected with the pRetroSuper expression plasmid (oligoengine) containing the shRNAs against PML and TRF2 (as described above) using calcium phosphate. In brief, 18 μg of DNA (pSUPER.retro constructs) were dissolved in 125mM $CaCl_2$ final concentration. HBS (50 mM Hepes, pH 7.1, 300 mM NaCl, 1.5 mM Na_2HPO_4) solution was gently vortexed and the DNA-$CaCl_2$ solution was added drop-wise. The solution was kept at room temperature for 30 min and then added drop wise to the cells seeded in a 10 cm dish and incubated 16 h at 37°C. The cells were extensively washed with PBS and then incubated in complete medium. Cells were selected with 1 μg/ml puromycin (Sigma-Aldrich). From pooled puromycin-resistant cells, individual colonies were isolated using 3-mm cloning discs (Sigma-Aldrich) folllowing the manufacturer's instructions, and passaged into medium containing 0.5 μg/ml puromycin. In bold are targeting sequences: *P-all* 5′-GATCCCCCGCCAGCCCAGAAGAGGAATTCAAGAGATTCCTCTTCTGGGCTGGCGTTTTT-3′ 3′-GGGGCGGTCGGGTCTTCTCCTTAAGTTCTCTAAGGAGAAGACCCGACCGCAAAAATTCGA-5′ TRF2 5′-GATCCCCGAGGATGAACTGTTTCAAGTTCAAGAGACTTGAAACAGTTCATCCTCTTTTT-3′ 3′-GGGCTCCTACTTGACAAAGTTCAAGTTCTCTGAACTTTGTCAAGTAGGAGAAAAATTCGA-5′

TET-On inducible TRF2

U2OS cells stably transfected with a TET-On plasmid were cultured in DME supplemented with 10% (vol/vol) heat inactivated TET-free FBS and 100 U/ml penicillin (GIBCO BRL) and 100 mg/ml streptomycin (GIBCO BRL). Cells were seeded in 150-mm dishes and transfected with the pSuperior expression plasmid (oligoengine) containing the shRNAs against TRF2 (as described above) using Effectene according to the manufacturers protocol (QIAGEN). In brief, 8 μg of DNA (pSuperior constructs), 1.2 ml Buffer EC, 32 μl Enhancer and 80 μl of Effectene were used. The cells were placed in selection 2 d after transfection in 1 μg/ml puromycin (Sigma-Aldrich). From pooled puromycin-resistant cells, individual colonies were isolated using 3-mm cloning discs (Sigma-Aldrich) as per the manufacturer's instructions, and passaged into medium containing 0.5 μg/ml puromycin: Cells were induced with 0.5 mg/ml doxycycline and screened for positive clones by Western blotting.

TRF2$^{\Delta B\Delta M}$ transient and stable transfection

U2OS cells were cotransfected with pBabePuro^{R}-NMycTRF2$^{\Delta B\Delta M}$ (derived from pLPC-NMycTRF2$^{\Delta B\Delta M}$, a gift from Dr. Titia De Lange, Rockefeller University, NY) and 1/6 (molar ratio) of GFP using Effectene according to the manufacturers protocol (QIAGEN). Cells were sorted for GFP in a Becton Dickinson FACS Vantage. Recovered cells were cultured in complete DME and 25 μg/ml Fungizone (Sigma-Aldrich) and collected at different time points after sorting for Western blotting, immunofluorescence and metaphase spreads. U2OS cells were transfected with pBabePuro^{R}-NMycTRF2$^{\Delta B\Delta M}$ placed in selection 2 d after transfection in 1 μg/ml puromicin (Sigma-Aldrich). From pooled puromicin-resistant cells, individual colonies were isolated using 3-mm cloning discs (Sigma-Aldrich) as per the manufacturer's instructions, and passaged into medium containing 0.8 μg/ml puromycin: Cells were screened for positive clones by Western blotting and immunofluorescence.

Colony forming assay

Cells were seeded in 10-cm dishes and transfected as described above. Alternatively, inducible shTRF2 clones were plated at different densities and treated with doxycycline or left untreated. Colony formation was determined by crystal violet staining 10 d after selection. In brief, plates were placed on ice and washed twice with ice-cold 1× PBS. Cells were then fixed with ice-cold methanol (stored at −20°C) for 10 min. Methanol was aspirated from the plates, and 0.5% crystal violet solution (made in 25% methanol and stored at room temperature) was added to cover bottom of plate and incubated at room temperature for 10 min. The crystal violet solution was poured off and the plates were carefully rinsed with distilled H_2O until no color came off in the rinse. Plates were left to air dry at room temperature and colony numbers were determined using GeneSnap and GeneTools from Syngene.

Western blotting

Cells were lysed directly in SDS-sample buffer or in modified RIPA lysis buffer containing 50 mM Tris pH 7.6, 150 mM sodium chloride, 0.5% Triton X-100, 2.5 mM sodium fluoride, 2 mM sodium orthovanadate and a cocktail of protease inhibitors. Samples were analyzed by SDS-PAGE, transferred onto a nitrocellulose membrane and probed with the relevant antibodies.

Immunofluorescence

Protein localization and expression were visualized by fluorescence microscopy. For this purpose, cells were grown on glass coverslips and fixed in 4% paraformaldehyde (PFA). After washing with PBS, cells were permeabilized using 0.1% Triton X-100 solution and blocked with 10% goat serum. Following incubation with the primary antibodies, cells were washed and incubated with fluorescently labeled secondary antibodies (Molecular Probes). Image acquisition and processing information: (1) Make and model of microscope: Zeiss Axiovert 200, Zeiss LSM510. (2) Type, magnification, and numerical aperture of the objective lenses: 40× plan neofluor NA1.3; 63× plan apochromat NA1.4. (3) Temperature: room temperature. (4) Imaging medium: Prolong Antifade kit (Invitrogen). (5) Fluorochromes; AlexaFluor 488, AlexaFluor 555/568, AlexaFluor 647 (Invitrogen). (6) Camera make and model: Hamamatsu OrcaER. (7) Acquisition software: Zeiss Confocal software, Openlab Improvision Z-stacks were generated in 0.4-μm step increments, and 3D reconstructions were performed using software (Volocity; Improvision, Inc.). Images were processed using Adobe Photoshop 7.0. (8) Images were

subsequently exported to TIFF. Figures were mounted using Adobe Photoshop and saved as JPEG files.

Hoechst staining
Cells were incubated with 2 μM Hoechst 33342, a cell-permeable nucleic acid stain, for 10 min and then analyzed by live microscopy. Snapshots of different fields were taken and mitoses (or apoptotic nuclei) analyzed.

PNA/FISH with IF
Cells were grown on coverslips and fixed with ice-cold methanol-acetic acid. They were then prepared as for immunofluorescence but were not mounted. After secondary antibody incubation, coverslips were washed in PBS 3 times for 5 min and post-fixed in 4% PFA for 2 min. After three quick rinses in PBS the coverslips were dehydrated in EtOH in series 70%, 85%, 96% for 2 min each. Coverslips were then completely air dried. FITC- or rhodamine-conjugated PNA probe (Panagene) stock was diluted 1:1,000 in hybridization solution (30% formamide, 0.1% Triton X-100, 0.3× SSC) and heated at 80°C for 3 min. Coverlips were then incubated in the dark at room temp for 30 min, rinsed in wash solution (4× SSC, 0.05% Tween 20) for 5 min. Cells were then counterstained with Dapi, mounted and stored at 4°C.

Apoptosis/cell cycle (PI staining)
To determine cell death PI staining and FACS analysis was performed. In brief, cells were fixed in 70% EtOH, spun, washed in PBS and spun again. The pellet was resuspended in 60 μl of PBS with 300 μg/ml RNase and incubated for 30 min at room temperature. 10 μg/ml of propidium iodide was then added and samples were incubated in the dark for 30 min before being analyzed through a Becton Dickinson FACS machine. DNA profiles were analyzed using the CellQuest acquisition/analysis software.

Cell size
Live cells were run through a Schaerfe System (Casy) machine and cell diameter was determined. Alternatively, cells were fixed with 70% EtOH and run through a BD FACS. Forward scatter (FSC-H) histograms of different clones were compared.

Senescence
Cells were fixed in 4% PFA and stained with the SA-βGal solution (5 mM potassium ferrocyanide, 5 mM potassium ferricyanide, 40 mM citric acid, 166 mM Na_2HPO_4, 40 mM NaH_2PO_4, 2 mM $MgCl_2$, 375 mM NaCl, 1 mg/ml X-Gal, pH 6.0) for 6–24 h. Cells were then analyzed by light microscopy.

Immunoprecipitation
Samples were collected and lysed in ice cold lysis buffer (50 mM Tris, pH 7.6, 150 mM sodium chloride, 0.5% Triton X-100, 2.5 mM sodium fluoride, and 2 mM sodium orthovanadate) with protease inhibitors. 500–1,000 μg of total protein, as determined by Bradford assays, was precleared and then incubated with 500 ng of Protein G agarose-conjugated antibody at 4°C for 3 h, followed by 1-h incubation with Sepharose beads. After five washes with ice-cold lysis buffer containing protease and phosphatase inhibitors, the immunoprecipitates were subjected to Western analysis as described above.

FlowFISH analysis
FlowFISH was performed following the protocol by Lansdrop and colleagues (Rufer et al., 1998).

Cytogenetic analysis
Cells were harvested for cytogenetic analysis using standard techniques. In brief, cells were arrested at metaphase with colcemid (final concentration 0.05 μg/ml 1–2 h). After detachment cells were treated with a hypotonic solution of KCl (0.075 M), fixed using 3:1 methanol/glacial acetic acid and slides prepared. Telomeres were detected using fluorescent in situ hybridization (FISH) to a to Rhodamine conjugated peptide nucleic acid (PNA) probe (Rho-OO-CCCTAACCCTAACCCTAA, PE Biosystems) or a similar PNA conjugated to FITC. PNA hybridization was conducted as described previously (Lansdorp et al., 1996; Zijlmans et al., 1997) and cells were counterstained with DAPI. Digital images were captured with the Smartcapture software (Digital Scientific) using a 63 or 100× objectives on a Zeiss Axioskop microscope fitted with a multiple filter wheel and suitable filters.

Genomic DNA extraction and Southern blot procedure
Genomic DNA was extracted from stable clones at various passages. In brief, 10^7 cells were trypsinized, washed and resuspended in 500 μl 1× SSC. Subsequently, 500 μl of 2× lysis buffer (100 mM Tris HCl, pH 7.5, 100 mM NaCl, 10 mM EDTA, and 1% Sarkosyl) were added together with 50 μg/ml of RNase, and the samples were left to stand at room temperature for 20 min before adding 500μg/ml of proteinase K and leaving them rotating overnight at 55°C. The samples were then subjected to phenol/chloroform extraction and subsequent ethanol precipitation. DNA concentration was measured using a spectrophotometer. Approximately 5μg of purified genomic DNA was digested with the restriction enzymes HinfI and RsaI (NEB). The digested DNA was quantified and 3.0 μg was loaded on a 1% agarose gel in 0.5× TBE. Samples were electrophoresed in a CHEF-DR III pulse-field electrophoresis apparatus (Bio-Rad Laboratories) in recirculating 0.5× TBE buffer at 14°C. Electrophoresis conditions were 5v per cm for 12 h with a 0.5–1.5 switch time. The gel was rinsed and stained with ethidium bromide to visualize the DNA and a Southern blot produced on Hybond N+ membrane using standard techniques. Southern blot membrane was hybridized to a ^{32}P-αdCTP labeled telomere probe in modified Church buffer (EDTA 1 mM, $NaHPO_4$, pH 7.2, 0.5 M SDS 7%) at 65°C and subsequently washed in 1.0×SSC, 0.1% SDS at 65°C. The blot was visualized using a PhosphorImager (Typhoon; GE Healthcare) and telomere length determined using the Telometric Software (Fox Chase Cancer Center, Philadelphia, PA). Subsequently the blots were hybridized to a ^{32}PαdCTP labeled MS1 minisatellite probe (Jeffreys et al., 1988) as loading control between tracks.

Online supplemental material
Figure S1 shows the effects of TRF2 RNAi or functional inhibition on cell viability and end-to-end fusions. Figure S2 shows the effect of TRF2 RNAi or functional inhibition on genomic stability and cell size. Figure S3 shows the effect of TRF2 RNAi on APBs. Figure S4 contains loading controls for TRF (A and B) and FlowFISH (C). Figure S5 shows ATM and ATM targets localization with respect to APBs in various ALT and telomerase-positive cell lines (A–D). Moreover, the figure contains an analysis of p53 expression and localization pattern in ALT and telomerase positive cells (E–I). Online supplemental material is available at http://www.jcb.org/cgi/content/full/jcb.200703020/DC1.

A special thanks to Cristian Bellodi in P.S. laboratory for critical discussion and technical assistance. We thank Dr Titia De Lange (Rockefeller University, New York, USA), Andrew Fry (University of Leicester, UK), Tina Rich (University of Glasgow, UK) and Roger Reddel (Cancer Research Unit, Westmead, Australia) for reagents. We also thank Gerry Cohen, Gerry Melino, Miguel Martins (MRC Toxicology Unit, Leicester, UK), Ed Louis, Gianni Liti (Department of Genetics, University of Nottingham, UK) and Melania Capasso (MRC Unit, Leicester, UK) for critical discussion.

P. Salomoni and M. Stagno D'Alcontres. are supported by the MRC, UK. N.J. Royle is recipient of an MRC grant. A. Mendez-Bermudez was funded by a PhD studentship from CONACYT (Mexico).

Submitted: 5 March 2007
Accepted: 1 November 2007

References

Bartkova, J., N. Rezaei, M. Liontos, P. Karakaidos, D. Kletsas, N. Issaeva, L.V. Vassiliou, E. Kolettas, K. Niforou, V.C. Zoumpourlis, et al. 2006. Oncogene-induced senescence is part of the tumorigenesis barrier imposed by DNA damage checkpoints. *Nature.* 444:633–637.

Bernardi, R., P.P. Scaglioni, S. Bergmann, H.F. Horn, K.H. Vousden, and P.P. Pandolfi. 2004. PML regulates p53 stability by sequestering Mdm2 to the nucleolus. *Nat. Cell Biol.* 6:665–672.

Bi, X., D. Srikanta, L. Fanti, S. Pimpinelli, R. Badugu, R. Kellum, and Y.S. Rong. 2005. Drosophila ATM and ATR checkpoint kinases control partially redundant pathways for telomere maintenance. *Proc. Natl. Acad. Sci. USA.* 102:15167–15172.

Blanco, R., P. Munoz, J.M. Flores, P. Klatt, and M.A. Blasco. 2007. Telomerase abrogation dramatically accelerates TRF2-induced epithelial carcinogenesis. *Genes Dev.* 21:206–220.

Brinkley, B.R. 2001. Managing the centrosome numbers game: from chaos to stability in cancer cell division. *Trends Cell Biol.* 11:18–21.

Bryan, T.M., A. Englezou, J. Gupta, S. Bacchetti, and R.R. Reddel. 1995. Telomere elongation in immortal human cells without detectable telomerase activity. *EMBO J.* 14:4240–4248.

de Lange, T. 2002. Protection of mammalian telomeres. *Oncogene.* 21:532–540.

de Lange, T. 2005. Shelterin: the protein complex that shapes and safeguards human telomeres. *Genes Dev.* 19:2100–2110.

de Stanchina, E., E. Querido, M. Narita, R.V. Davuluri, P.P. Pandolfi, G. Ferbeyre, and S.W. Lowe. 2004. PML is a direct p53 target that modulates p53 effector functions. *Mol. Cell.* 13:523–535.

Di Micco, R., M. Fumagalli, A. Cicalese, S. Piccinin, P. Gasparini, C. Luise, C. Schurra, M. Garre, P.G. Nuciforo, A. Bensimon, et al. 2006. Oncogene-induced senescence is a DNA damage response triggered by DNA hyper-replication. *Nature.* 444:638–642.

Jeffreys, A.J., N.J. Royle, V. Wilson, and Z. Wong. 1988. Spontaneous mutation rates to new length alleles at tandem-repetitive hypervariable loci in human DNA. *Nature.* 332:278–281.

Jiang, W.Q., Z.H. Zhong, J.D. Henson, and R.R. Reddel. 2007. Identification of candidate alternative lengthening of telomeres genes by methionine restriction and RNA interference. *Oncogene.* 26:4635–4647.

Karlseder, J., D. Broccoli, Y. Dai, S. Hardy, and T. de Lange. 1999. p53- and ATM-dependent apoptosis induced by telomeres lacking TRF2. *Science.* 283:1321–1325.

Karlseder, J., A. Smogorzewska, and T. de Lange. 2002. Senescence induced by altered telomere state, not telomere loss. *Science.* 295:2446–2449.

Karlseder, J., K. Hoke, O.K. Mirzoeva, C. Bakkenist, M.B. Kastan, J.H. Petrini, and T. Lange Td. 2004. The telomeric protein TRF2 binds the ATM kinase and can inhibit the ATM-dependent DNA damage response. *PLoS Biol.* 2:E240.

Kirsch-Volders, M., A. Vanhauwaert, M. De Boeck, and I. Decordier. 2002. Importance of detecting numerical versus structural chromosome aberrations. *Mutat. Res.* 504:137–148.

Lansdorp, P.M., N.P. Verwoerd, F.M. van de Rijke, V. Dragowska, M.T. Little, R.W. Dirks, A.K. Raap, and H.J. Tanke. 1996. Heterogeneity in telomere length of human chromosomes. *Hum. Mol. Genet.* 5:685–691.

Londono-Vallejo, J.A., H. Der-Sarkissian, L. Cazes, S. Bacchetti, and R.R. Reddel. 2004. Alternative lengthening of telomeres is characterized by high rates of telomeric exchange. *Cancer Res.* 64:2324–2327.

Mallette, F.A., M.F. Gaumont-Leclerc, and G. Ferbeyre. 2007. The DNA damage signaling pathway is a critical mediator of oncogene-induced senescence. *Genes Dev.* 21:43–48.

Mihara, K., M. Iijima, T. Kondo, and M. Namba. 1996. Selective expression of mutated p53 in human cells immortalized with either 4-nitroquinoline 1-oxide or 60Co gamma rays. *Cell Struct. Funct.* 21:111–116.

Munoz, P., R. Blanco, J.M. Flores, and M.A. Blasco. 2005. XPF nuclease-dependent telomere loss and increased DNA damage in mice overexpressing TRF2 result in premature aging and cancer. *Nat. Genet.* 37:1063–1071.

Muntoni, A., and R.R. Reddel. 2005. The first molecular details of ALT in human tumor cells. *Hum. Mol. Genet.* 14:R191–R196.

Naka, K., K. Ikeda, and N. Motoyama. 2002. Recruitment of NBS1 into PML oncogenic domains via interaction with SP100 protein. *Biochem. Biophys. Res. Commun.* 299:863–871.

Oh, B.K., Y.J. Kim, C. Park, and Y.N. Park. 2005. Up-regulation of telomere-binding proteins, TRF1, TRF2, and TIN2 is related to telomere shortening during human multistep hepatocarcinogenesis. *Am. J. Pathol.* 166:73–80.

Pearson, M., R. Carbone, C. Sebastiani, M. Cioce, M. Fagioli, S. Saito, Y. Higashimoto, E. Appella, S. Minucci, P.P. Pandolfi, and P.G. Pelicci. 2000. PML regulates p53 acetylation and premature senescence induced by oncogenic Ras. *Nature.* 406:207–210.

Potts, P.R., and H. Yu. 2007. The SMC5/6 complex maintains telomere length in ALT cancer cells through SUMOylation of telomere-binding proteins. *Nat. Struct. Mol. Biol.* 14:581–590.

Razak, Z.R., R.J. Varkonyi, M. Kulp-McEliece, C. Caslini, J.R. Testa, M.E. Murphy, and D. Broccoli. 2004. p53 differentially inhibits cell growth depending on the mechanism of telomere maintenance. *Mol. Cell. Biol.* 24:5967–5977.

Rufer, N., W. Dragowska, G. Thornbury, E. Roosnek, and P.M. Lansdorp. 1998. Telomere length dynamics in human lymphocyte subpopulations measured by flow cytometry. *Nat. Biotechnol.* 16:743–747.

Salomoni, P., and P.P. Pandolfi. 2002. The role of PML in tumor suppression. *Cell.* 108:165–170.

Takai, H., A. Smogorzewska, and T. de Lange. 2003. DNA damage foci at dysfunctional telomeres. *Curr. Biol.* 13:1549–1556.

van Steensel, B., A. Smogorzewska, and T. de Lange. 1998. TRF2 protects human telomeres from end-to-end fusions. *Cell.* 92:401–413.

Verdun, R.E., and J. Karlseder. 2006. The DNA damage machinery and homologous recombination pathway act consecutively to protect human telomeres. *Cell.* 127:709–720.

Verdun, R.E., L. Crabbe, C. Haggblom, and J. Karlseder. 2005. Functional human telomeres are recognized as DNA damage in G2 of the cell cycle. *Mol. Cell.* 20:551–561.

Wang, R.C., A. Smogorzewska, and T. de Lange. 2004. Homologous recombination generates T-loop-sized deletions at human telomeres. *Cell.* 119:355–368.

Wu, G., W.H. Lee, and P.L. Chen. 2000. NBS1 and TRF1 colocalize at promyelocytic leukemia bodies during late S/G2 phases in immortalized telomerase-negative cells. Implication of NBS1 in alternative lengthening of telomeres. *J. Biol. Chem.* 275:30618–30622.

Wu, G., X. Jiang, W.H. Lee, and P.L. Chen. 2003. Assembly of functional ALT-associated promyelocytic leukemia bodies requires Nijmegen Breakage Syndrome 1. *Cancer Res.* 63:2589–2595.

Xu, L., and E.H. Blackburn. 2004. Human Rif1 protein binds aberrant telomeres and aligns along anaphase midzone microtubules. *J. Cell Biol.* 167:819–830.

Yeager, T.R., A.A. Neumann, A. Englezou, L.I. Huschtscha, J.R. Noble, and R.R. Reddel. 1999. Telomerase-negative immortalized human cells contain a novel type of promyelocytic leukemia (PML) body. *Cancer Res.* 59:4175–4179.

Zhu, X.D., B. Kuster, M. Mann, J.H. Petrini, and T. de Lange. 2000. Cell-cycle-regulated association of RAD50/MRE11/NBS1 with TRF2 and human telomeres. *Nat. Genet.* 25:347–352.

Zijlmans, J.M., U.M. Martens, S.S. Poon, A.K. Raap, H.J. Tanke, R.K. Ward, and P.M. Lansdorp. 1997. Telomeres in the mouse have large inter-chromosomal variations in the number of T2AG3 repeats. *Proc. Natl. Acad. Sci. USA.* 94:7423–7428.